Available online at www.sciencedirect.com
SCIENCE DIRECT®
Journal of Sound and Vibration 276 (2004) 593–613
JOURNAL OF SOUND AND VIBRATION
www.elsevier.com/locate/jsvi

Equivalent acoustic impedance model. Part 2: analytical approximation

B. Faverjon, C. Soize*

Laboratoire de Mécanique, Université de Marne-La-Vallée, 5 boulevard Descartes, 2 77454 Marne-La-Vallée Cedex, France

Received 10 February 2003; accepted 4 August 2003

Abstract

In the context of the prediction of noise levels in vibroacoustic systems, numerical models or analytical models can be developed. Generally, numerical models are adapted to the low and medium frequency ranges and analytical models to the medium and high frequency ranges. For analytical models, a classical approximation consists of modelling the multilayer system by an equivalent acoustic impedance. This paper deals with a multilayer system consisting of a porous medium inserted between two thin plates. Part 1 of this paper is devoted to the experiments performed and to the development of a probabilistic algebraic model for the equivalent acoustic impedance. In the present Part 2, an analytical method is constructed for this multilayer system. This method consists of introducing the unbounded medium in the plane directions x_1 and x_2 while the medium is bounded in the x_3-direction. A two-dimensional space Fourier transform introducing the wave vector co-ordinates k_1 and k_2 is used. For a given frequency and for k_1 and k_2 fixed, the boundary value problem in x_3 consists of 12 differential equations in x_3 whose coefficients depend on k_1 and k_2, with boundary conditions. This system of equations is solved by using adapted algebraic calculations. By inverse Fourier transform with respect to k_1 and k_2, the equivalent acoustic impedance is deduced. The method which is proposed is not usual. Finally, a comparison of this analytical approach is compared with the experimental results.

1. Introduction

Soundproofing schemes usually used for acoustic insulation consist of a single porous medium layer or several inserted between plates. Much research has already been devoted to the vibro-acoustics of simple structures such as beams, plates, circular cylindrical shells, coupled with

*Corresponding author. Tel.: +33-1-60-95-77-91; fax: +33-1-60-95-77-99.
E-mail address: soize@univ-mlv.fr (C. Soize).

0022-460X/$ - see front matter © 2003 Elsevier Ltd. All rights reserved.
doi:10.1016/j.jsv.2003.08.054

internal or external acoustic fluids, by analytical methods (for instance see Refs. [1–8]) and to the vibro-acoustics of general structures by numerical methods (see for instance [5,9]). Concerning the vibro-acoustics of multilayer systems without porous medium, a large number of works were published (for instance see Refs. [2,5,10–16]). The difficulties of modelling multilayer systems are due to the problems induced by the acoustic behaviour of porous media and by the coupling between the layers constituting the system. The porous medium is a complex material consisting of two phases: one fluid and one solid. The dissipation inside a porous medium is induced by viscous effects (friction of the fluid phase to the solid phase on the pore walls), by thermal effects (absorption of the remaining heat from the fluid phase by the solid phase) and by structural damping related to the viscoelasticity of the solid phase. A porous medium can be modelled by an equivalent fluid model [17–19] if the assumption of a motionless solid phase can be justified. If the fluid phase is strongly coupled with the solid phase or, if the porous medium is coupled with a vibrating structure, one needs to take into account the motion of the solid phase [1,20–29]. The coupling between the different layers of a multilayer system is obtained by the construction of the interface conditions between the layers (see for instance Refs. [24,30–32]).

Acoustic transmission through porous media or multilayer systems including porous media have recently been studied using the finite element method. In this context, the entire system includes porous media which are discretized by finite elements [33–41]. These methods are very efficient in the low-frequency range, have to be adapted to be efficient in the medium frequency range and cannot be used at high frequencies in the present state of the art. For simple structures, analytical methods can be used for the medium and high frequency ranges (see for instance Refs. [24,42–48]).

In this paper, for the medium and high frequency ranges, one presents the modelling of a multilayer system with porous medium by an analytical approach in order to construct an equivalent acoustic impedance of this multilayer system. Such an acoustic impedance model can be used for the prediction of vibro-acoustic responses of complex systems, allowing such a soundproofing scheme to be modelled. The multilayer system under consideration consists of a three-dimensional porous medium made of an open polyurethane foam inserted between two thin plates. This system is described in Part 1 [49] of the paper.

Concerning the three-dimensional porous medium, a three-dimensional formulation is used and is based on the Biot theory which introduces the displacement fields associated with the solid and the fluid phases. The motion of the solid phase cannot be neglected because the porous medium is inserted between two vibrating plates. Equations are written in the general case of a homogeneous anisotropic porous medium whose solid phase is viscoelastic. In order to solve the equations, the two in-plane components of the fluid phase displacement are eliminated and the third one component relative to the thickness direction is preserved. The boundary value problem of the multilayer system is constructed by using the local equations of plates, for bending and membrane deformations, coupled with the three-dimensional porous medium. Since the multilayer system corresponds to one three-dimensional medium coupled with two two-dimensional media, the interface conditions between the layers have to be constructed. Such a method was presented in Ref. [50] for the case of a plate in bending mode coupled with a three-dimensional elastic media. In this paper, an extension to the case of the above multilayer system is presented [51].

For the multilayer system under consideration, the construction of the acoustic impedance operator and its local approximation (introduced in Part 1 [49]) is carried out using an analytical method for which the finite reference-plane of the mechanical system is replaced by an infinite reference-plane. This kind of approximation is *a priori* usable for the medium and high frequency ranges. This analytical method uses the spatial co-ordinate corresponding to the thickness direction and uses a two-dimensional spatial Fourier transform for the two directions corresponding to the reference plane which is infinite. For a given frequency and for each wave vector associated with the reference-plane directions, a system of differential equations with respect to the thickness direction with appropriate boundary conditions has to be solved. This system consists of twelve coupled equations: three for each plate (two for the membrane deformation and one for the bending deformation), six for the porous medium (three for the solid phase and three for the fluid phase). This system of equations is partially degenerate. Consequently, the elimination of the two in-plane phase fluid displacements can be performed and, then coupled equations deduced ten. This system of equations has bad numerical conditioning induced by the presence of terms which exponentionally increase in the thickness direction of the porous medium. An adapted method has specifically been developed in order to solve such a system of differential equations.

Concerning the validation of this analytical method by using the experimental results introduced in Part 1 [49], the mechanical properties corresponding to the experiment are used. Consequently, one has to consider a homogeneous isotropic porous medium with a viscoelastic solid phase and two homogeneous viscoelastic isotropic plates. The analytical method is then developed in this context. The parameters of the porous medium introduced in the Biot theory, applied in the context of acoustic problems [22–24], were measured [52,53]. The complete set of the anisotropic porous medium parameters has not been measured. Consequently, the measured parameters only allow the isotropic and transverse isotropic case to be described. The main objective of this paper is the experimental validation of the analytical model for a porous medium modelled by a homogeneous isotropic porous medium with a viscoelastic solid phase. The transverse isotropic viscoelastic solid phase is studied in [51]. Nevertheless, a comparison between the isotropic and transverse isotropic cases is presented for the local acoustic impedance.

In Section 2, the boundary value problem is given considering the general case of a homogeneous anisotropic viscoelastic porous medium coupled with two homogeneous orthotropic viscoelastic plates in membrane and bending deformations. In Section 3, using the two-dimensional inplane space Fourier transform, the boundary value problem is deduced. Section 4 deals with the construction of the equivalent acoustic impedance. The experimental validation is presented in Section 5.

2. Expression of the boundary value problem

The Love-Kirchhoff model is used for the bending motions of the two plates called P_1 and P_2 and the membrane motions are considered. Let Ω be the three-dimensional bounded region occupied by the porous material. The interfaces between the porous medium and the plates P_1 and P_2 are denoted by Σ_1 and Σ_2 (see Fig. 1). A pressure field p is applied to Σ_0. Let S_1 and S_2 be the mid-planes of the plates P_1 and P_2. The co-ordinates (x_1, x_2, x_3) of a point belonging to the porous

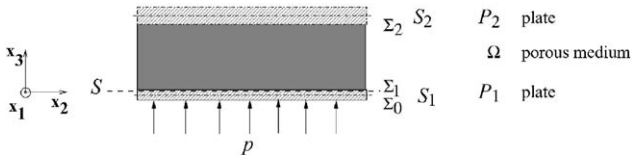

Fig. 1. Geometry of the multilayer system.

medium are given in the Cartesian system whose origin belongs to the reference-plane S of the multilayer system which is chosen as the coupling interface Σ_1. Consequently, surface S coincides with surface Σ_1. The x_3 co-ordinate of the coupling interface Σ_1 (or Σ_2) is 0 (or H) (in which H is the thickness of the porous medium). In this paper, if $\mathscr{T}$ is any quantity depending on the co-ordinates x_1, x_2 and x_3, $\mathscr{T}_{,k}$ denotes the partial derivative $\partial\mathscr{T}/\partial x_k$ and $\mathscr{T}' = \partial\mathscr{T}/\partial x_3$, $\mathscr{T}'' = \partial^2\mathscr{T}/\partial x_3^2$. The Kronecker symbol denoted by $\delta_{\alpha\beta}$ is such that $\delta_{\alpha\beta} = 1$ for $\alpha = \beta$, $\delta_{\alpha\beta} = 0$ for $\alpha \neq \beta$.

2.1. Membrane and bending vibrations equations for plates P_1 and P_2

Using thin plate classical hypotheses for plate P_ℓ, $\ell = 1, 2$ and since the Love-Kirchhoff model is used for the bending motions of the two plates and the membrane motions are added, the displacement field of plate P_ℓ, $\ell = 1, 2$, is defined by $(v_1^{P_\ell}(x_1, x_2), v_2^{P_\ell}(x_1, x_2), w^{P_\ell}(x_1, x_2))$ where $v_1^{P_\ell}(x_1, x_2)$ and $v_2^{P_\ell}(x_1, x_2)$ are the inplane displacements (membrane displacements) of plate P_ℓ and $w^{P_\ell}(x_1, x_2)$ is its transverse displacement. Plate P_1 is submitted to a pressure field p. The boundary value problem is written as follows. The dynamical equations of plate P_1 for bending and membrane motions are expressed as

$$-\omega^2 \rho_{P_1} h_{P_1} v_\alpha^{P_1} - N_{\alpha\beta,\beta}^{P_1} = \sigma_{\alpha 3}^{1s} \quad \text{on } S_1, \tag{1}$$

$$-\omega^2 \rho_{P_1} h_{P_1} w^{P_1} - M_{\alpha\beta,\alpha\beta}^{P_1} = \sigma_{33}^{1s} + \sigma_{33}^{1f} + h_{P_1}\sigma_{\alpha 3,\alpha}^{1s}/2 + p \quad \text{on } S_1, \tag{2}$$

in which the solid part stress tensor components σ_{ij}^s and the fluid part stress tensor components σ_{ij}^f are defined by

$$\sigma_{ij}^{1s}(x_1, x_2) = \sigma_{ij}^s(x_1, x_2, 0), \quad \sigma_{ij}^{1f}(x_1, x_2) = \sigma_{ij}^f(x_1, x_2, 0). \tag{3}$$

The dynamical equations of plate P_2 for bending and membrane motions are given by

$$-\omega^2 \rho_{P_2} h_{P_2} v_\alpha^{P_2} - N_{\alpha\beta,\beta}^{P_2} = -\sigma_{\alpha 3}^{2s} \quad \text{on } S_2, \tag{4}$$

$$-\omega^2 \rho_{P_2} h_{P_2} w^{P_2} - M_{\alpha\beta,\alpha\beta}^{P_2} = -\sigma_{33}^{2s} - \sigma_{33}^{2f} + h_{P_2}\sigma_{\alpha 3,\alpha}^{2s}/2 \quad \text{on } S_2, \tag{5}$$

in which

$$\sigma_{ij}^{2s}(x_1, x_2) = \sigma_{ij}^s(x_1, x_2, H), \quad \sigma_{ij}^{2f}(x_1, x_2) = \sigma_{ij}^f(x_1, x_2, H), \tag{6}$$

The right-hand side of Eqs. (1), (2), (4) and (5) correspond to the coupling effects of the three-dimensional porous medium on the plates. For orthotropic plate P_ℓ with $\ell = 1, 2$, the components of the bending moment tensor $M_{\alpha\beta}^{P_\ell}$ and the components of the inplane force tensor $N_{\alpha\beta}^{P_\ell}$ are

written as

$$M_{\alpha\beta}^{P_\ell} = -(1 + \mathrm{i}\omega a_1^{P_\ell}(\omega)) D_{P_\ell}^f [\nu^{P_\ell} w_{,\gamma\gamma}^{P_\ell} \delta_{\alpha\beta} + (1 - \nu^{P_\ell}) w_{,\alpha\beta}^{P_\ell}], \tag{7}$$

$$N_{\alpha\beta}^{P_\ell} = (1 + \mathrm{i}\omega a_1^{P_\ell}(\omega)) D_{P_\ell}^m \left[\nu^{P_\ell} v_{\gamma,\gamma}^{P_\ell} \delta_{\alpha\beta} + \tfrac{1}{2}(1 - \nu^{P_\ell})(v_{\alpha,\beta}^{P_\ell} + v_{\beta,\alpha}^{P_\ell})\right], \tag{8}$$

in which $D_{P_\ell}^f = E^{P_\ell} h_{P_\ell}^3/[12(1 - \nu^{P_\ell 2})]$, $D_{P_\ell}^m = E^{P_\ell} h_{P_\ell}/[1 - \nu^{P_\ell 2}]$.

2.2. Three-dimensional vibrations of the porous medium

Let $\mathbf{u}^s = (u_1^s, u_2^s, u_3^s)$ and $\mathbf{u}^f = (u_1^f, u_2^f, u_3^f)$ be the displacement field of the solid phase and the fluid phase, respectively, for the porous medium. The dynamical equations of the porous medium for the solid part and the fluid part are the Biot equations [22–24] and are written as

$$-\omega^2 \tilde{\rho}_{11} u_i^s - \omega^2 \tilde{\rho}_{12} u_i^f - \mathrm{i}\omega \Phi^2 [\mathbb{k}^{-1}]_{ij} (u_j^f - u_j^s) - \tilde{\sigma}_{ij,j}^s = 0 \quad \text{in } \Omega, \tag{9}$$

$$-\omega^2 \tilde{\rho}_{22} u_i^f - \omega^2 \tilde{\rho}_{12} u_i^s + \mathrm{i}\omega \Phi^2 [\mathbb{k}^{-1}]_{ij} (u_j^f - u_j^s) - \tilde{\sigma}_{ij,j}^f = 0 \quad \text{in } \Omega, \tag{10}$$

in which $\mathbb{k}$ is the permeability tensor relative to viscous effects and Φ is the porosity. The coefficients $\tilde{\rho}_{11}$, $\tilde{\rho}_{22}$ and $\tilde{\rho}_{12}$ are the density of the solid phase, the density of the fluid phase and the coupling density between the solid and the fluid phases, respectively. For k and l equal to 1 or 2, $\tilde{\rho}_{kl}$ is defined by [35]

$$\tilde{\rho}_{kl}(\omega) = \rho_{kl} + \Delta\rho_{kl}(\omega), \tag{11}$$

in which an expression of $\Delta\rho_{kl}(\omega)$ is given in Section 3 and where

$$\rho_{11} = \rho_1 + \Phi\rho_f(\alpha - 1), \quad \rho_{22} = \Phi\rho_f\alpha, \quad \rho_{12} = -\Phi\rho_f(\alpha - 1), \tag{12}$$

with $\rho_1 = (1 - \Phi)\rho_s$ and where α is the tortuosity, ρ_f the fluid mass density and ρ_s the solid material mass density.

The boundary conditions between the porous medium and plate P_ℓ are given by writing the continuity of the normal displacement for the fluid phase and the continuity of the displacement field for the solid phase, that is to say

$$\begin{aligned} u_\alpha^s &= v_\alpha^{P_1} - \frac{h_{P_1}}{2} w_{,\alpha}^{P_1}, \quad u_3^s = w^{P_1}, \quad u_3^f = w^{P_1} \quad \text{on } \Sigma_1, \\ u_\alpha^s &= v_\alpha^{P_2} + \frac{h_{P_2}}{2} w_{,\alpha}^{P_2}, \quad u_3^s = w^{P_2}, \quad u_3^f = w^{P_2} \quad \text{on } \Sigma_2. \end{aligned} \tag{13}$$

Since the porous medium is assumed to be viscoelastic and anisotropic, the constitutive equations are given by

$$\sigma_{ij}^s(\mathbf{x}, \omega) = (L_{ijkh}^s(\omega) + \mathrm{i}\omega D_{ijkh}(\omega))\varepsilon_{kh}^s + L_{ijkh}^{sf}(\omega)\varepsilon_{kh}^f, \tag{14}$$

$$\sigma_{ij}^f(\mathbf{x}, \omega) = L_{ijkh}^f(\omega)\varepsilon_{kh}^f + L_{ijkh}^{fs}(\omega)\varepsilon_{kh}^s, \tag{15}$$

$$\begin{aligned} L_{ijkh}^s(\omega) &= A_{ijkh}(\omega) + M(\omega)[B_{ij}B_{kh} - \Phi(B_{ij}\delta_{kh} + \delta_{ij}B_{kh}) + \Phi^2\delta_{ij}\delta_{kh}], \\ L_{ijkh}^f(\omega) &= M(\omega)\Phi^2\delta_{ij}\delta_{kh}, \quad L_{ijkh}^{sf}(\omega) = L_{ijkh}^{fs}(\omega) = M(\omega)\Phi(B_{ij}\delta_{kh} - \Phi\delta_{ij}\delta_{kh}), \end{aligned} \tag{16}$$

in which ε^s_{kh} and ε^f_{kh} are the strain tensors relative to the solid phase and the fluid phase, respectively. The components $A_{ijkh}(\omega)$ and $D_{ijkh}(\omega)$ are relative to the elastic stress tensor and to the damping stress tensor, respectively. The two tensors have the usual symmetric properties and are positive definite [9]. If one considers a hysteretic damping, the components $D_{ijkh}(\omega)$ can be written as $D_{ijkh}(\omega) = a_1(\omega)A_{ijkh}(\omega)$ in which $a_1(\omega)$ is a real positive constant which depends on ω. The B_{ij} components are relative to the coupling of the solid phase with the fluid phase. The thermal effects are expressed by $M(\omega)$ which is defined by $M(\omega) = K_e(\omega)/\Phi$ in which $K_e(\omega)$ is the frequency dependent equivalent complex bulk modulus of air [24] and is given by

$$K_e(\omega) = \frac{K_a}{\gamma - \dfrac{\gamma - 1}{1 + 8\eta_f/(\mathrm{i}\Lambda'^2 P_r \omega \rho_f) G'(\omega)}}, \tag{17}$$

where K_a is the bulk modulus of the fluid (in case of air, $K_a = \gamma p_f$, where p_f is the pressure), η_f, the fluid viscosity, P_r, the Prandtl number, Λ', the thermal characteristic length [24,39] which has to be identified experimentally, $G'(\omega)$, the complex factor defined by [24]

$$G'(\omega) = \sqrt{1 + \mathrm{i}\omega/\omega_{Tt}}, \tag{18}$$

with $\omega_{Tt} = 16\eta_f/(P_r\Lambda'^2\rho_f) > 0$ is real.

3. Boundary value problem in the Fourier space

As explained in Section 1, and in order to compare this analytical prediction with the experiments, the porous medium is considered as a homogeneous viscoelastic isotropic medium and the plates are considered as homogeneous viscoelastic isotropic media. This model can easily be extended to the case of an anisotropic porous medium whose equations are given in Section 2. The method proposed for the construction of the equivalent acoustic impedance is based on the spectral method relative to the infinite plane $(x_1 O x_2)$ containing the reference-plane S of the multilayer system. Since the thickness H is finite, the co-ordinate x_3, corresponding to the thickness direction, is preserved (see Fig. 2). In order to simplify the notation, a function and its Fourier transform are denoted by the same symbol and differ by their arguments. Let $\tilde{\mathbf{x}} = (x_1, x_2)$ be the point in reference-plane S of the multilayer system, $\mathbf{k} = (k_1, k_2)$, $\mathrm{d}\tilde{\mathbf{x}} = \mathrm{d}x_1\,\mathrm{d}x_2$ and $\mathrm{d}\mathbf{k} = \mathrm{d}k_1\,\mathrm{d}k_2$. The Fourier transform $g(\mathbf{k}, \omega)$ of a function $\tilde{\mathbf{x}} \mapsto g(\tilde{\mathbf{x}}, \omega)$ with respect to $\tilde{\mathbf{x}}$ is such that

$$g(\mathbf{k}, \omega) = \int_{\mathbb{R}^2} \mathrm{e}^{\mathrm{i}\mathbf{k}\cdot\tilde{\mathbf{x}}} g(\tilde{\mathbf{x}}, \omega)\,\mathrm{d}\tilde{\mathbf{x}}, \quad g(\tilde{\mathbf{x}}, \omega) = \frac{1}{(2\pi)^2} \int_{\mathbb{R}^2} \mathrm{e}^{-\mathrm{i}\mathbf{k}\cdot\tilde{\mathbf{x}}} g(\tilde{\mathbf{k}}, \omega)\,\mathrm{d}\mathbf{k}, \tag{19}$$

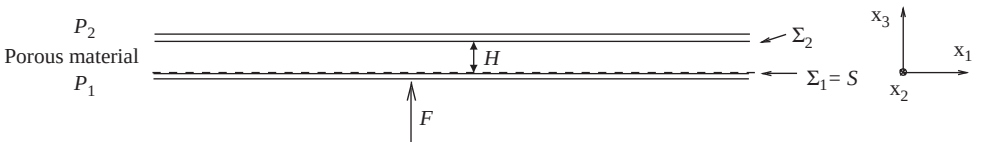

Fig. 2. Infinite multilayer system in plane (x_1, x_2).

with $\mathbf{k}\cdot\tilde{\mathbf{x}} = k_1x_1 + k_2x_2$. The derivative $\partial w/\partial x_3$ is denoted by w'. The Fourier transforms with respect to (x_1, x_2) of the dynamical equations for the solid and the fluid phases of the porous medium are

$$\begin{aligned} &-\omega^2\tilde{\rho}_{11}u_i^s - \omega^2\tilde{\rho}_{12}u_i^f - \mathrm{i}\omega b(u_i^f - u_i^s) + \mathrm{i}k_1\sigma_{i1}^s + \mathrm{i}k_2\sigma_{i2}^s - \sigma_{i3,3}^s = 0,\\ &-\omega^2\tilde{\rho}_{22}u_i^f - \omega^2\tilde{\rho}_{12}u_i^s + \mathrm{i}\omega b(u_i^f - u_i^s) - \sigma_{i3,3}^f = 0, \end{aligned} \tag{20}$$

in which $b(\omega) = \Phi^2/\mathcal{K}(\omega)$ where $\mathcal{K}(\omega)$ is the permeability for the isotropic case. The coefficient $b(\omega)$ is relative to the viscous effects and is written as [22–24,35]

$$b(\omega) = \Phi^2\sigma G_R(\omega), \tag{21}$$

in which $G_R(\omega) > 0$ with $G_R(-\omega) = G_R(\omega)$ is the real part of $G(\omega) = \sqrt{1 + \mathrm{i}P\hat{\omega}/2}$ which is the viscous corrective factor, and where $P = 8\alpha k_0/(\Phi\Lambda^2)$ with $k_0 = \eta_f/\sigma$, the viscous static permeability, and where $\sigma > 0$ is the resistivity which has to be identified experimentally. The non-dimensional factor $\hat{\omega}$ is defined by $\hat{\omega} = \omega\alpha\rho_f k_0/(\Phi\eta_f)$ and the viscous characteristic length Λ has to be identified experimentally. The added mass $\Delta\rho_{kl}(\omega)$, introduced in Eq. (11), due to viscous effects, is defined by Panneton [35]

$$\Delta\rho_{kl}(\omega) = (-1)^{k+l}\Phi^2\sigma G_I(\omega)/\omega, \tag{22}$$

where $G_I(\omega)$ is the imaginary part of $G(\omega)$ and which has to verify these following algebraic properties [51]

$$G_I(\omega) > 0 \quad \text{for } \omega > 0, \quad G_I(-\omega) = -G_I(\omega), \quad \lim_{\omega\to 0}|G_I(\omega)/\omega| = C < \infty, \tag{23}$$

in which C is a finite constant. An expression of $G_I(\omega)$ is given by [24]

$$G_I(\omega) = \frac{1}{\sqrt{2}}\frac{\omega/\omega_{Tv}}{\sqrt{1 + \sqrt{1 + (\omega/\omega_{tv})^2}}}, \tag{24}$$

in which $\omega_{Tv} = \sigma^2\Lambda^2\Phi^2/(4\alpha^2\eta_s\rho_f)$ where the structural dissipation factor η_s has to be identified experimentally. For the solid phase of the porous medium, the Fourier transforms with respect to (x_1, x_2) of the constitutive equations are

$$\begin{aligned} \sigma_{11}^s(\mathbf{k}, x_3, \omega) &= A_F(\omega)(-\mathrm{i}k_1u_1^s - \mathrm{i}k_2u_2^s + u_{3,3}^s) + B_F(\omega)(-\mathrm{i}k_1)u_1^s\\ &\quad + C_F(\omega)(-\mathrm{i}k_1u_1^f - \mathrm{i}k_2u_2^f + u_{3,3}^f),\\ \sigma_{22}^s(\mathbf{k}, x_3, \omega) &= A_F(\omega)(-\mathrm{i}k_1u_1^s - \mathrm{i}k_2u_2^s + u_{3,3}^s) + B_F(\omega)(-\mathrm{i}k_2)u_2^s\\ &\quad + C_F(\omega)(-\mathrm{i}k_1u_1^f - \mathrm{i}k_2u_2^f + u_{3,3}^f),\\ \sigma_{33}^s(\mathbf{k}, x_3, \omega) &= A_F(\omega)(-\mathrm{i}k_1u_1^s - \mathrm{i}k_2u_2^s + u_{3,3}^s) + B_F(\omega)u_{3,3}^s\\ &\quad + C_F(\omega)(-\mathrm{i}k_1u_1^f - \mathrm{i}k_2u_2^f + u_{3,3}^f),\\ \sigma_{12}^s(\mathbf{k}, x_3, \omega) &= -\mathrm{i}B_F(\omega)(k_2u_1^s + k_1u_2^s)/2,\\ \sigma_{13}^s(\mathbf{k}, x_3, \omega) &= B_F(\omega)(u_{1,3}^s - \mathrm{i}k_1u_3^s)/2,\\ \sigma_{23}^s(\mathbf{k}, x_3, \omega) &= B_F(\omega)(u_{2,3}^s - \mathrm{i}k_2u_3^s)/2, \end{aligned} \tag{25}$$

in which $A_F(\omega)$, $B_F(\omega)$ and $C_F(\omega)$ are defined by $A_F(\omega) = (1 + \mathrm{i}\omega a_1(\omega))vE/[(1+v)(1-2v)] + M(\omega)(B-\Phi)^2$, $B_F(\omega) = (1 + \mathrm{i}\omega a_1(\omega))E/(1+v)$, $C_F(\omega) = \Phi M(\omega)(B-\Phi)$ with E, the Young modulus and v the Poisson coefficient of the solid phase. In acoustic problems, the coupling factor B is such that $B = 1$ [22,24]. For the fluid phase, the Fourier transforms with respect to (x_1, x_2) of the constitutive equations are

$$\sigma_{ii}^f(\mathbf{k}, x_3, \omega) = E_F(\omega)(-\mathrm{i}k_1 u_1^f - \mathrm{i}k_2 u_2^f + u_{3,3}^f) + C_F(\omega)(-\mathrm{i}k_1 u_1^s - \mathrm{i}k_2 u_2^s + u_{3,3}^s), \tag{26}$$

for $i = 1, 2, 3$, and where $E_F(\omega) = \Phi^2 M(\omega)$. The plate P_1 is subjected to a point force applied to the origine of plate P_1 in the direction x_3 with the intensity $f(\omega)$. Therefore, the pressure field p introduced in Eq. (2) is such that $p(\tilde{\mathbf{x}}, \omega) = f(\omega)\delta_0(\tilde{\mathbf{x}})$ in which $\delta_0(\tilde{\mathbf{x}})$ is the Dirac function at point 0. For plates P_1 and P_2, the Fourier transforms with respect to (x_1, x_2) of the dynamical equations are

$$\begin{aligned} &-\omega^2 \rho_{P_1} h_{P_1} \mathbf{u}^{P_1} + (1 + \mathrm{i}\omega a_1^{P_1}(\omega))\mathbb{K}_1(\mathbf{k})\mathbf{u}^{P_1} = \mathbf{F}_1(\mathbf{k}, \omega) + \mathbf{f}(\omega), \\ &-\omega^2 \rho_{P_2} h_{P_2} \mathbf{u}^{P_2} + (1 + \mathrm{i}\omega a_1^{P_2}(\omega))\mathbb{K}_2(\mathbf{k})\mathbf{u}^{P_2} = \mathbf{F}_2(\mathbf{k}, \omega), \end{aligned} \tag{27}$$

in which $\mathbf{u}^{P_1}(\mathbf{k}, \omega) = (v_1^{P_1}(\mathbf{k}, \omega), v_2^{P_1}(\mathbf{k}, \omega), w^{P_1}(\mathbf{k}, \omega))$ and $\mathbf{u}^{P_2}(\mathbf{k}, \omega) = (v_1^{P_2}(\mathbf{k}, \omega), v_2^{P_2}(\mathbf{k}, \omega), w^{P_2}(\mathbf{k}, \omega))$, $\mathbf{f}(\omega)$ is such that $\mathbf{f}(\omega) = (0, 0, f(\omega))$, for $\ell = 1$ or 2, $\mathbb{K}_\ell(\mathbf{k})$ is the stiffness matrix for plate P_ℓ and is such that

$$\mathbb{K}_\ell(\mathbf{k}) = \begin{bmatrix} a_{11}^\ell(\mathbf{k}) & a_{12}^\ell(\mathbf{k}) & 0 \\ a_{12}^\ell(\mathbf{k}) & a_{22}^\ell(\mathbf{k}) & 0 \\ 0 & 0 & a_{33}^\ell(\mathbf{k}) \end{bmatrix}, \tag{28}$$

in which

$$\begin{aligned} &a_{11}^\ell(\mathbf{k}) = D_{P_\ell}^m[(1+v^{P_\ell})k_1^2 + (1-v^{P_\ell})(k_1^2+k_2^2)]/2, \quad a_{12}^\ell(\mathbf{k}) = D_{P_\ell}^m(1+v^{P_\ell})k_1k_2/2, \\ &a_{22}^\ell(\mathbf{k}) = D_{P_\ell}^m[(1+v^{P_\ell})k_2^2 + (1-v^{P_\ell})(k_1^2+k_2^2)]/2, \quad a_{33}^\ell(\mathbf{k}) = D_{P_\ell}^f(k_1^2+k_2^2)^2. \end{aligned} \tag{29}$$

The vectors $\mathbf{F}_1(\mathbf{k}, \omega)$ and $\mathbf{F}_2(\mathbf{k}, \omega)$ correspond to the forces induced by the porous medium on the plates P_1 and P_2 and are given by

$$\mathbf{F}_1(\mathbf{k}, \omega) = \begin{bmatrix} \sigma_{13}^{1s} \\ \sigma_{23}^{1s} \\ \sigma_{33}^{1s} + \tilde{\sigma}_{33}^{1f} - \mathrm{i}h_{P_1}(k_1\sigma_{13}^{1s} + k_2\sigma_{23}^{1s})/2 \end{bmatrix},$$

$$\mathbf{F}_2(\mathbf{k}, \omega) = \begin{bmatrix} -\sigma_{13}^{2s} \\ -\sigma_{23}^{2s} \\ -\sigma_{33}^{2s} - \sigma_{33}^{2f} - \mathrm{i}h_{P_2}(k_1\sigma_{13}^{2s} + k_2\sigma_{23}^{2s})/2 \end{bmatrix}. \tag{30}$$

Finally, the boundary value problem in x_3 is completely defined in adding the Fourier transform with respect to (x_1, x_2) of the boundary conditions defined by Eq. (13), i.e.

$$\begin{aligned} &u_\alpha^s = v_\alpha^{P_1} + \mathrm{i}h_{P_1}k_\alpha w^{P_1}/2, \quad u_3^s = w^{P_1}, \quad u_3^f = w^{P_1}, \quad \text{on } \Sigma_1, \quad \alpha = 1, 2, \\ &u_\alpha^s = v_\alpha^{P_2} - \mathrm{i}h_{P_2}k_\alpha w^{P_2}/2, \quad u_3^s = w^{P_2}, \quad u_3^f = w^{P_2}, \quad \text{on } \Sigma_2. \end{aligned} \tag{31}$$

4. Solving the boundary value problem and calculation of the equivalent acoustic impedance

For ω, k_1 and k_2 fixed, the boundary value problem in x_3, constructed in Section 3, consists of 12 coupled differential equations in x_3 whose coefficients depend on ω, k_1 and k_2, and on boundary conditions. The acoustic impedance equivalent to the multilayer system being assumed homogeneous in plane $\tilde{\mathbf{x}} = (x_1, x_2)$, the pressure field p applied to plate P_1 is related to the normal velocity jump $\Delta v(\tilde{\mathbf{x}}', \omega) = v^{P_1}(\tilde{\mathbf{x}}', \omega) - v^{P_2}(\tilde{\mathbf{x}}', \omega)$, with $v^{P_1}(\tilde{\mathbf{x}}', \omega) = \mathrm{i}\omega w^{P_1}(\tilde{\mathbf{x}}', \omega)$ and $v^{P_2}(\tilde{\mathbf{x}}', \omega) = \mathrm{i}\omega w^{P_2}(\tilde{\mathbf{x}}', \omega)$, and is given by the following equation (see Part 1 of the paper):

$$p(\tilde{\mathbf{x}}, \omega) = \int_{\tilde{\mathbf{x}}' \in S} z(\tilde{\mathbf{x}} - \tilde{\mathbf{x}}', \omega) \Delta v(\tilde{\mathbf{x}}', \omega) \, \mathrm{d}S_{\tilde{\mathbf{x}}'}, \quad \tilde{\mathbf{x}} \in S, \tag{32}$$

where $\mathrm{d}S_{\tilde{\mathbf{x}}'} = \mathrm{d}x_1' \, \mathrm{d}x_2'$. The Fourier transform with respect to $\tilde{\mathbf{x}}$ of Eq. (32) is written as

$$p(\mathbf{k}, \omega) = \mathrm{i}\omega z(\mathbf{k}, \omega) \Delta w(\mathbf{k}, \omega), \tag{33}$$

in which $\Delta w(\mathbf{k}, \omega) = w^{P_1}(\mathbf{k}, \omega) - w^{P_2}(\mathbf{k}, \omega)$ is the Fourier transform of $\Delta w(\tilde{\mathbf{x}}, \omega) = w^{P_1}(\tilde{\mathbf{x}}, \omega) - w^{P_2}(\tilde{\mathbf{x}}, \omega)$. An equation allowing the calculation of $p(\mathbf{k}, \omega)$ as a function of $\Delta w(\mathbf{k}, \omega)$ has to be constructed. Consequently, the unknowns $\mathbf{u}^f$ and $\mathbf{u}^s$ have to be eliminated from the system of equations. Substituting Eqs. (25) and (26) into Eq. (20) yields

$$\begin{bmatrix} \mathbb{A}_{11} & 0 \\ 0 & 0 \end{bmatrix} \begin{bmatrix} \mathbf{X}''(x_3) \\ \mathbf{Y}''(x_3) \end{bmatrix} + \begin{bmatrix} \mathbb{B}_{11}(\mathbf{k}) & \mathbb{B}_{12}(\mathbf{k}) \\ \mathbb{B}_{12}^{\mathrm{T}}(\mathbf{k}) & 0 \end{bmatrix} \begin{bmatrix} \mathbf{X}'(x_3) \\ \mathbf{Y}'(x_3) \end{bmatrix} + \begin{bmatrix} \mathbb{C}_{11}(\mathbf{k}) & \mathbb{C}_{12}(\mathbf{k}) \\ \mathbb{C}_{12}^{\mathrm{T}}(\mathbf{k}) & \mathbb{C}_{22}(\mathbf{k}) \end{bmatrix} \begin{bmatrix} \mathbf{X}(x_3) \\ \mathbf{Y}(x_3) \end{bmatrix} = 0, \tag{34}$$

for x_3 in $[0, H]$, in which vectors $\mathbf{X}(x_3)$ and $\mathbf{Y}(x_3)$ are such that $\mathbf{X}(x_3) = (u_1^s(x_3), u_2^s(x_3), u_3^s(x_3), u_3^f(x_3))$ and $\mathbf{Y}(x_3) = (u_1^f(x_3), u_2^f(x_3))$. It should be noted that all quantities in Eq. (34) depend on ω. In order to simplify the notation, the dependence on $\mathbf{k}$ of $\mathbf{X}$ and $\mathbf{Y}$ is omitted. The matrices $\mathbb{A}_{11}$, $\mathbb{B}_{11}(\mathbf{k})$, $\mathbb{B}_{12}(\mathbf{k})$, $\mathbb{C}_{11}(\mathbf{k})$, $\mathbb{C}_{12}(\mathbf{k})$ and $\mathbb{C}_{22}(\mathbf{k})$ are defined in Appendix A and $\mathbb{A}^{\mathrm{T}}$ is the transpose of matrix $\mathbb{A}$. Since $\mathbb{C}_{22}(\mathbf{k})$ is invertible for $\omega \neq 0$, $\mathbf{Y}$ can be eliminated from Eq. (34) by using the second line of this equation and yields

$$\mathbf{A}(\mathbf{k})\mathbf{X}''(x_3) + \mathbf{B}(\mathbf{k})\mathbf{X}'(x_3) + \mathbb{C}(\mathbf{k})\mathbf{X}(x_3) = 0, \tag{35}$$

in which $\mathbf{A}(\mathbf{k})$, $\mathbf{B}(\mathbf{k})$ and $\mathbb{C}(\mathbf{k})$ are defined by

$$\begin{aligned} \mathbf{A}(\mathbf{k}) &= \mathbb{A}_{11} - \mathbb{B}_{12}(\mathbf{k})\mathbb{C}_{22}^{-1}(\mathbf{k})\mathbb{B}_{12}^{\mathrm{T}}(\mathbf{k}), \\ \mathbf{B}(\mathbf{k}) &= \mathbb{B}_{11}(\mathbf{k}) - \mathbb{B}_{12}(\mathbf{k})\mathbb{C}_{22}^{-1}(\mathbf{k})\mathbb{C}_{12}^{\mathrm{T}}(\mathbf{k}) - \mathbb{C}_{12}(\mathbf{k})\mathbb{C}_{22}^{-1}(\mathbf{k})\mathbb{B}_{12}^{\mathrm{T}}(\mathbf{k}), \\ \mathbf{C}(\mathbf{k}) &= \mathbb{C}_{11}(\mathbf{k}) - \mathbb{C}_{12}(\mathbf{k})\mathbb{C}_{22}^{-1}(\mathbf{k})\mathbb{C}_{12}^{\mathrm{T}}(\mathbf{k}). \end{aligned} \tag{36}$$

One introduces $\mathbf{W}(x_3) = (\mathbf{X}'(x_3), \mathbf{X}(x_3))$. As above, the dependence in $\mathbf{k}$ and ω of $\mathbf{W}$ is omitted. The second-order differential equation (35) is transformed into the following first order differential equation

$$-\mathscr{A}(\mathbf{k})\mathbf{W}'(x_3) + \mathscr{B}(\mathbf{k})\mathbf{W}(x_3) = 0, \tag{37}$$

in which complex symmetric matrices $\mathscr{A}(\mathbf{k})$ and $\mathscr{B}(\mathbf{k})$ are such that

$$\mathscr{A}(\mathbf{k}) = \begin{bmatrix} -\mathbf{A}(\mathbf{k}) & 0 \\ 0 & \mathbf{C}(\mathbf{k}) \end{bmatrix} \quad \text{and} \quad \mathscr{B}(\mathbf{k}) = \begin{bmatrix} \mathbf{B}(\mathbf{k}) & \mathbf{C}(\mathbf{k}) \\ \mathbf{C}(\mathbf{k}) & 0 \end{bmatrix}. \tag{38}$$

In order to solve Eq. (37) and since it can be proved that the complex matrix $\mathscr{A}(\mathbf{k})^{-1}\mathscr{B}(\mathbf{k})$ is diagonalizable for any $\mathbf{k}$ in $\mathbb{R}^2$, the eigenvalue problem $\mathscr{A}(\mathbf{k})^{-1}\mathscr{B}(\mathbf{k})\Phi(\mathbf{k}) = \Phi(\mathbf{k})\Lambda(\mathbf{k})$ associated with this equation is introduced, in which $\Lambda(\mathbf{k})$ is the diagonal matrix constituted of the eight complex eigenvalues $\lambda_1, \ldots, \lambda_8$. The complex square matrix $\Phi(\mathbf{k})$ is constituted of the associated eigenvectors. Therefore, the general solution of Eq. (37) is written as

$$\mathbf{W}(x_3) = \mathscr{G}(\mathbf{k}, x_3)\mathbf{W}(0), \quad \mathscr{G}(\mathbf{k}, x_3) = \Phi(\mathbf{k})\mathscr{D}(\mathbf{k}, x_3)\Phi(\mathbf{k})^{-1},$$
$$[\mathscr{D}(\mathbf{k}, x_3)]_{jk} = \delta_{jk}\mathrm{e}^{x_3\lambda_j(\mathbf{k})}, \tag{39}$$

Taking $x_3 = H$ in Eq. (39), the vector $(\mathbf{X}'(H), \mathbf{X}'(0))$ can be expressed as a function of the vector $(\mathbf{X}(H), \mathbf{X}(0))$ which is written as

$$\begin{bmatrix} \mathbf{X}'(H) \\ \mathbf{X}'(0) \end{bmatrix} = \mathbb{M}_H(\mathbf{k}, \omega) \begin{bmatrix} \mathbf{X}(H) \\ \mathbf{X}(0) \end{bmatrix}, \tag{40}$$

in which the construction of the complex matrix $\mathbb{M}_H(\mathbf{k}, \omega)$ is given in Appendix B. It should be noted that the construction of the matrix $\mathbb{M}_H(\mathbf{k}, \omega)$ cannot be obtained by a direct algebraic calculation. This matrix has to be constructed using a numerical calculation on an ill-conditioned numerical problem. Consequently, an adapted algebraic calculation has to be developed in order to avoid the bad numerical conditioning. This ill-conditioning is due to the four complex eigenvalues having positive real parts while the four other complex eigenvalues with negative real parts do not induce numerical problems. These numerical difficulties are induced by the fact that, for x_3 in $[0, H]$, four diagonal terms of the matrix $\mathscr{D}(\mathbf{k}, x_3)$ are exponentionally increasing. In Appendix B, a well-conditioned formulation is constructed and consists of treating separately the two groups of eigenvalues. Using the second line of Eq. (34) with $\mathbf{X}'(0)$ and $\mathbf{X}'(H)$, and substituting Eq. (40) in the resulting equations yields

$$\begin{bmatrix} \mathbf{Y}(H) \\ \mathbf{Y}(0) \end{bmatrix} = (\mathbb{C}_B(\mathbf{k}, \omega)\mathbb{M}_H(\mathbf{k}, \omega) + \mathbb{C}_C(\mathbf{k}, \omega)) \begin{bmatrix} \mathbf{X}(H) \\ \mathbf{X}(0) \end{bmatrix}, \tag{41}$$

in which $\mathbb{C}_B(\mathbf{k}, \omega)$ and $\mathbb{C}_C(\mathbf{k}, \omega)$ are given by

$$\mathbb{C}_B(\mathbf{k}, \omega) = \begin{bmatrix} -\mathbb{C}_{22}(\mathbf{k}, \omega)^{-1}\mathbb{B}_{12}(\mathbf{k}, \omega)^{\mathrm{T}} & \mathbf{0} \\ \mathbf{0} & -\mathbb{C}_{22}(\mathbf{k}, \omega)^{-1}\mathbb{B}_{12}(\mathbf{k}, \omega)^{\mathrm{T}} \end{bmatrix},$$

$$\mathbb{C}_C(\mathbf{k}, \omega) = \begin{bmatrix} -\mathbb{C}_{22}(\mathbf{k}, \omega)^{-1}\mathbb{C}_{12}(\mathbf{k}, \omega)^{\mathrm{T}} & \mathbf{0} \\ \mathbf{0} & -\mathbb{C}_{22}(\mathbf{k}, \omega)^{-1}\mathbb{C}_{12}(\mathbf{k}, \omega)^{\mathrm{T}} \end{bmatrix}. \tag{42}$$

The boundary conditions defined by Eq. (31) can be rewritten as

$$\mathbf{X}(0) = \mathbb{L}_1(\mathbf{k})\mathbf{u}^{P_1} \quad \text{and} \quad \mathbf{X}(H) = \mathbb{L}_2(\mathbf{k})\mathbf{u}^{P_2}, \tag{43}$$

in which matrices $\mathbb{L}_1(\mathbf{k})$ and $\mathbb{L}_2(\mathbf{k})$ are defined by

$$\mathbb{L}_1(\mathbf{k}) = \begin{bmatrix} 1 & 0 & \mathrm{i}h_{P_1}k_1/2 \\ 0 & 1 & \mathrm{i}h_{P_1}k_2/2 \\ 0 & 0 & 1 \\ 0 & 0 & 1 \end{bmatrix}, \quad \mathbb{L}_2(\mathbf{k}) = \begin{bmatrix} 1 & 0 & -\mathrm{i}h_{P_2}k_1/2 \\ 0 & 1 & -\mathrm{i}h_{P_2}k_2/2 \\ 0 & 0 & 1 \\ 0 & 0 & 1 \end{bmatrix}. \tag{44}$$

Consequently, the vector $(\mathbf{F}_2(\mathbf{k},\omega),\mathbf{F}_1(\mathbf{k},\omega))$, in which $\mathbf{F}_2(\mathbf{k},\omega)$ and $\mathbf{F}_1(\mathbf{k},\omega)$ are defined by Eq. (30), can be rewritten as

$$\begin{bmatrix} \mathbf{F}_2(\mathbf{k},\omega) \\ \mathbf{F}_1(\mathbf{k},\omega) \end{bmatrix} = \mathbb{N}(\mathbf{k},\omega) \begin{bmatrix} \mathbf{u}^{P_2}(\mathbf{k},\omega) \\ \mathbf{u}^{P_1}(\mathbf{k},\omega) \end{bmatrix}, \tag{45}$$

where the matrix $\mathbb{N}(\mathbf{k},\omega)$ is a (6×6) complex matrix which can easily be calculated [51]. Substituting Eq. (45) into Eq. (27) allows the vector $(\mathbf{u}^{P_2}(\mathbf{k},\omega),\mathbf{u}^{P_1}(\mathbf{k},\omega))$ to be calculated as a function of $\mathbf{f}(\omega)$ by solving the linear matrix equation

$$\mathbb{P}(\mathbf{k},\omega) \begin{bmatrix} \mathbf{u}^{P_2}(\mathbf{k},\omega) \\ \mathbf{u}^{P_1}(\mathbf{k},\omega) \end{bmatrix} = \begin{bmatrix} \mathbf{0} \\ \mathbf{f}(\omega) \end{bmatrix}, \tag{46}$$

in which $\mathbb{P}(\mathbf{k},\omega)$ can easily be constructed. Knowing $\mathbf{u}^{P_1}(\mathbf{k},\omega)$ and $\mathbf{u}^{P_2}(\mathbf{k},\omega)$, one can deduce $w^{P_1}(\mathbf{k},\omega)$ and $w^{P_2}(\mathbf{k},\omega)$ and consequently, $\Delta w(\mathbf{k},\omega)$ which is equal to $w^{P_1}(\mathbf{k},\omega) - w^{P_2}(\mathbf{k},\omega)$ can be calculated by

$$\Delta w(\mathbf{k},\omega) = h(\mathbf{k},\omega) f(\omega), \tag{47}$$

in which $h(\mathbf{k},\omega) = [\mathbb{P}^{-1}(\mathbf{k},\omega)]_{66} - [\mathbb{P}^{-1}(\mathbf{k},\omega)]_{36}$. Taking the inverse Fourier transform in $\mathbf{k}$ of Eq. (47) yields

$$\Delta w(\tilde{\mathbf{x}},\omega) = h(\tilde{\mathbf{x}},\omega) f(\omega) \quad \text{with} \quad h(\tilde{\mathbf{x}},\omega) = \frac{1}{(2\pi)^2} \int_{\mathbb{R}^2} \mathrm{e}^{-\mathrm{i}\mathbf{k}\cdot\tilde{\mathbf{x}}} h(\mathbf{k},\omega)\,\mathrm{d}\mathbf{k}. \tag{48}$$

The equivalent acoustic impedance of the multilayer system being assumed isotropic in reference plane S, then $z(\tilde{\mathbf{x}}-\tilde{\mathbf{x}}',\omega)$ depends on $\|\tilde{\mathbf{x}}-\tilde{\mathbf{x}}'\|$ and consequently, the Fourier transform $z(\mathbf{k},\omega)$ depends on $\|\mathbf{k}\|$. One then deduces that $h(\mathbf{k},\omega)$ depends only on $k = \|\mathbf{k}\|$ and is rewritten as $h(k,\omega)$. Consequently, since the driving force is a point force applied to the origin, $\Delta w(\tilde{\mathbf{x}},\omega)$ depends only on $r = \|\tilde{\mathbf{x}}\|$ and is rewritten as $\Delta w(r,\omega)$. Thus $\omega \mapsto \Delta w(r,\omega)$ appears as the cross-frequency response function relative to two points distinct of r. Using the classical formula of the Fourier transform in polar co-ordinates yields

$$\Delta w(r,\omega) = \frac{1}{2\pi} \int_0^{+\infty} k\mathrm{J}_0(kr) h(k,\omega)\,\mathrm{d}k, \tag{49}$$

in which $\mathrm{J}_0(kr)$ is the zero order Bessel function. Eq. (49) gives a continuous expression of $\Delta w(r,\omega)$ as a function of the distance r between the origin in the reference-plane S and the point $\tilde{\mathbf{x}}$ in the reference-plane S. In order to compare the present model with the experiments (see Part 1 of the paper [49]), the (25×25) impedance matrix corresponding to the 25 driving and receiving points

has to be constructed. Let $[\Delta W(\omega)]$ be the (25×25) symmetric complex matrix defined by

$$[\Delta W(\omega)]_{jk} = \Delta w(r_{jk}, \omega), \tag{50}$$

in which $r_{jk} = \|\tilde{\mathbf{x}}_j - \tilde{\mathbf{x}}_k\|$ where $\tilde{\mathbf{x}}_1, \ldots, \tilde{\mathbf{x}}_{25}$ are the 25 driving points with a unite force and the receiving points defined in Fig. 2 of Part 1 of the paper. Consequently $[\Delta \mathbf{W}(\omega)]$ can be viewed as the matrix-valued frequency response function relative to these points. Let $[\mathbf{Z}(\omega)]$ be the corresponding (25×25) symmetric complex impedance matrix which is thus defined by

$$[\mathbf{Z}(\omega)] = \frac{1}{\mathrm{i}\omega}[\Delta W(\omega)]^{-1}. \tag{51}$$

For each ω fixed, complex matrix $[\mathbf{Z}(\omega)]$ is numerically calculated by using the analytical calculation presented above and in Appendices A and B. For ω belonging to the frequency band of analysis, impedance matrix $[\mathbf{Z}(\omega)]$ has to be compared to experimental impedance matrix $[\mathbf{Z}^{exp}(\omega)]$ constructed in Part 1 of the paper [49].

5. Experimental comparisons and validation

In this section, the analytical model is compared to the experiment presented in Part 1 of the paper. The geometry and the material properties of the multilayer system are given in Appendix A of Part 1 of the paper [49].

5.1. Experimental comparisons and validation for the equivalent acoustic impedance

The right-hand side of Eq. (49) is numerically calculated with a space step $\Delta r = 6.28 \times 10^{-3}$ m for r in $[0, 6.3]$ m.

5.1.1. Local acoustic impedance

The analytical model of the local equivalent acoustic impedance corresponds to the diagonal terms of the impedance matrix defined by Eq. (51). Figs. 3–5 display the graphs of the real part and the imaginary part of the local equivalent acoustic impedance at the points 8, 15 and 16, defined in Fig. 2 of Part 1 [49]. The solid lines are relative to the analytical model and the dashed lines to the experiments. There is a good agreement between the analytical model and the experimental results for these three points but also for all the other 22 points (see Ref. [51]), which are not presented in this paper. Since the results for all the 25 points cannot be given in the present paper, and taking into account that the graphs of all the real parts are similar and that the graphs of all the imaginary parts are similar, a part of the results can be synthesized in giving the real part and the imaginary part of the average local acoustic impedance defined as $\frac{1}{25}\sum_{j=1}^{25}[\mathbf{Z}(\omega)]_{jj}$. Concerning this average local impedance, Figs. 6(a) and (b) compare the analytical results with the experiments for the real part and for the imaginary part. On each figure, there is a good agreement between analytical result and experiment. In Figs. 3 to 6, it can be seen that the real parts (see Figs. 3(a), 4(a), 5(a) and 6(a)) and the imaginary parts (see Figs. 3(b), 4(b), 5(b) and 6(b)) of the impedance look similar to the schematic graph given in Fig. 6 of Part 1, that is to say, for all $\omega \geqslant 0$, the real part is positive with a peak at 844 Hz, and the imaginary part has a vertical

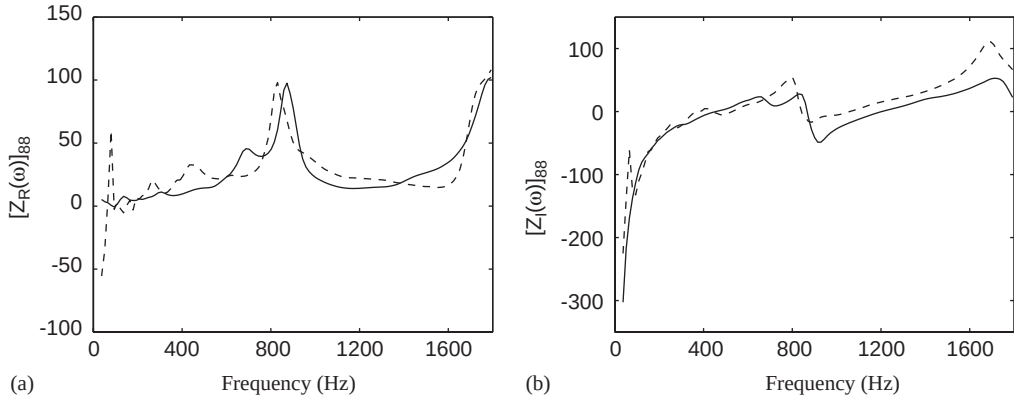

Fig. 3. (a) Real and (b) imaginary parts of the local equivalent acoustic impedance at the point 8. Analytical model (solid line), experimental results (dashed line).

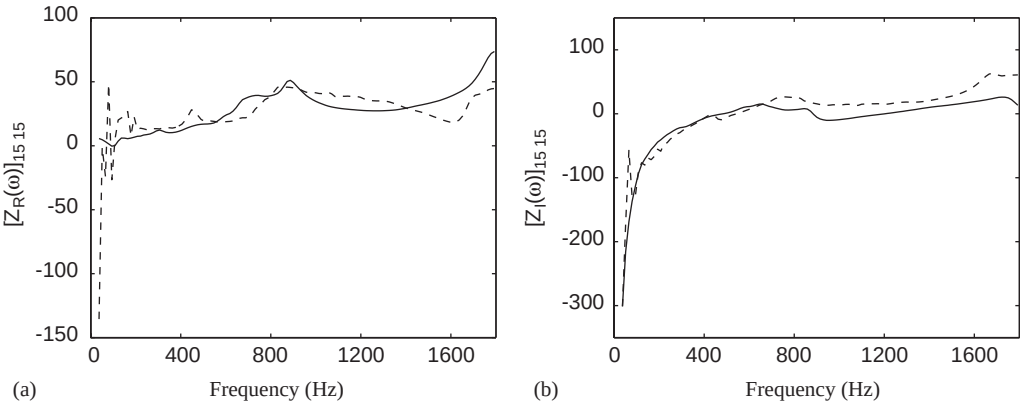

Fig. 4. (a) Real and (b) imaginary parts of the local equivalent acoustic impedance at the point 15. Key as for Fig. 3.

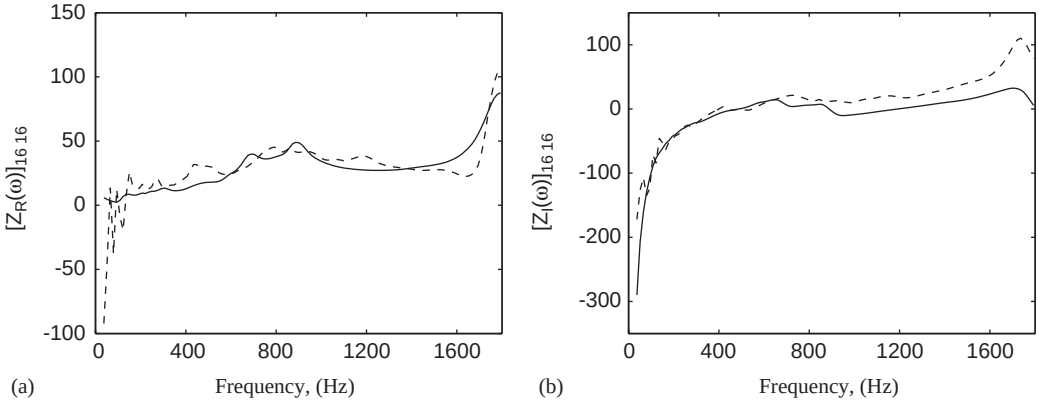

Fig. 5. (a) Real and (b) imaginary parts of the local equivalent acoustic impedance at the point 16. Key as for Fig. 3.

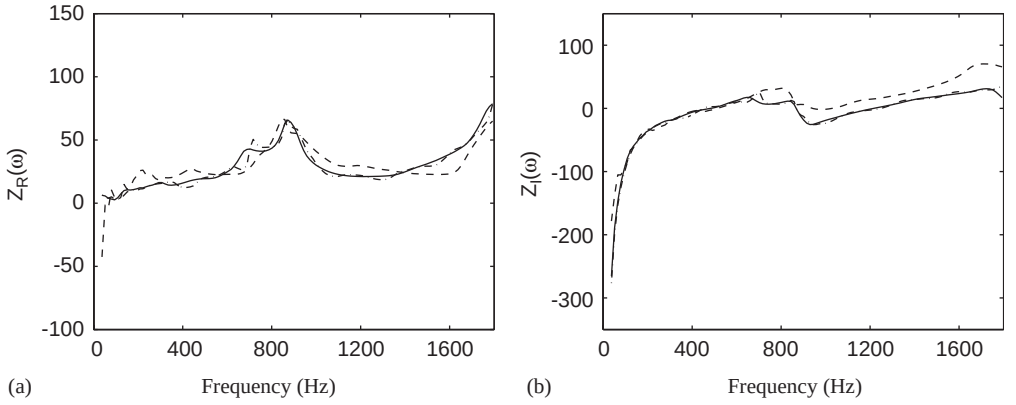

Fig. 6. (a) Real and (b) imaginary parts of the average local equivalent acoustic impedance on all points. Analytical model for isotropic solid phase (solid line), experimental results (dashed line), analytical model for transverse isotropic phase (dash-dot line).

asymptote when ω goes to 0 and there is a zero crossing for a frequency equal to 400 Hz associated with the peak of the real part. The peak and the associated zero crossing seem to be due to a resonance phenomenum between the dilatational wave which preferentially propagates in the fluid phase of the porous medium and the bending waves in the two plates. In addition, Figs. 6(a) and (b) compare the analytical results for an isotropic porous medium (solid line) with the analytical results for a porous medium having a transverse isotropic solid phase (dash-dot line) whose parameters have been partially measured [53]. One can observe that these two analytical models are very similar. Consequently, in this paper, one only presents results for the case of an isotropic porous medium. For the case of a transverse isotropic solid phase of the porous medium, theory details and results can be found in Ref. [51]. The robustness of the analytical method has been proved by performing a sensitivity analysis with respect to the parameters of the solid phase (mass density, Young modulus, dissipation factor and Poisson coefficient) and of the coupling between the two phases (porosity, tortuosity, resistivity, viscous and thermal characteristic lengths). From this sensitivity analysis, it can be concluded that the analytical model weakly depends on these parameters. For instance, Figs. 7 and 8 show the results for the Poisson ratio ν varying in [0.25, 0.46] and for the resistivity σ varying in $[2000, 20000]$ N s m^{-4}. Figs. 7a and 8a display the real part of the impedance, Figs. 7b and 8b display its imaginary part.

It should be noted that, although the averaged impedance does not seem affected by the resistivity, other numerical simulations have been performed in Ref. [51]. For instance, the porous medium has been modelled by the fluid equivalent theory. Such a model does not give good results with respect to the experiments. In order to study the type of model for the porous medium, the parametric analysis performed in Ref. [51] shows that the complete 3D model of the porous medium presented in this paper is necessary to predict the experimental results with a good accuracy.

5.1.2. Off-diagonal terms of the acoustic impedance

The equivalent acoustic impedance tends to become local for frequencies greater than 300 Hz. Figs. 9(a) and (b) display the equivalent acoustic impedance as a function of distance r between

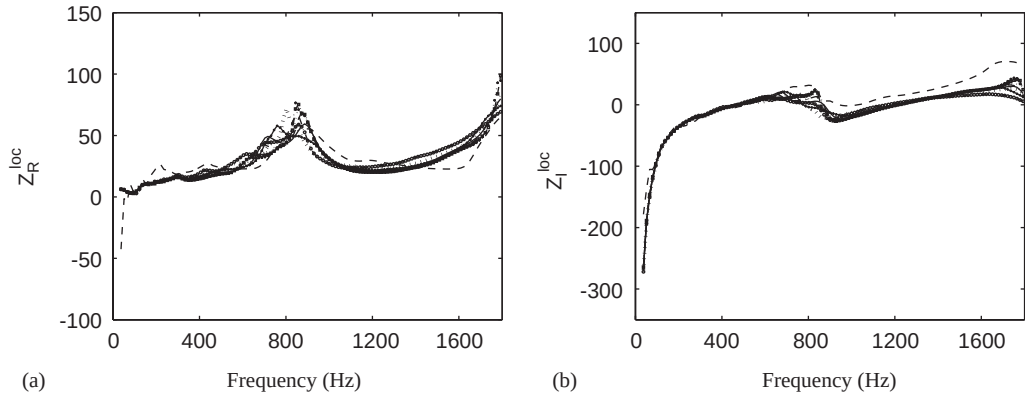

Fig. 7. (a) Real and (b) imaginary parts of the average local equivalent acoustic impedance over all the points for the different values of the Poisson coefficient v (from 0.25 to 0.46). Experimental results for Z_R (dashed line), predicted values of acoustic impedance for varying Poisson coefficient v: 0.25 (dotted line with asterisk symbols), 0.28 (dashed line with square symbols), 0.31 (dotted line), 0.34 (dash-dot line), 0.37 (solid line), 0.4 (solid line with cross symbols), 0.43 (thick dotted line), 0.46 (dash-dot line with circle symbols).

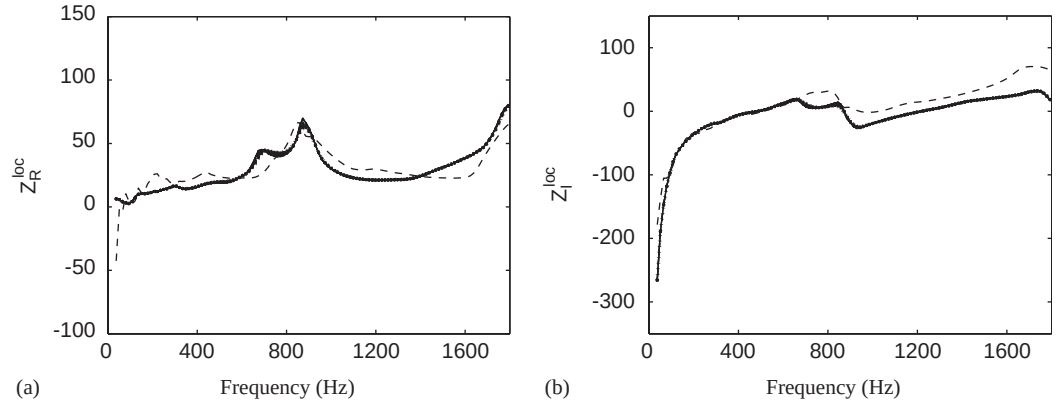

Fig. 8. (a) Real and (b) imaginary parts of the average local equivalent acoustic impedance over all the points for the different values of the resistivity σ (N s m^{-4}). Experimental results (dashed line), predicted results: 2000 (solid line), 4000 (solid line with cross symbols), 6000 (dotted line), 8000 (dash-dot line), 10 000 (dashed line with circle symbols), 12 000 (dash-dot line with circle symbols), 14 000 (dotted line with circle symbols), 16 000 (dashed line with asterisk symbols), 18 000 (dotted line with square symbols), 20 000 (thick dotted line).

the driving and the receiving points. For a frequency equal to 1400 Hz, the analytical results (circle symbols) and the experimental results (cross symbols) are very close. This conclusion holds for the other frequencies (see Ref. [51]). The aspect of the real part (Fig. 9(a)) and of the imaginary part (Fig. 9(b)) of the equivalent acoustic impedance as a function of the distance r has been explained in Part 1 [49] (exponential decreasing, sinusoidal function, non-zero phase for $\omega = 0$ for the imaginary part). For the other frequencies belonging to [300, 1600] Hz, the results are very similar. There is a good agreement between the analytical results and the experiments.

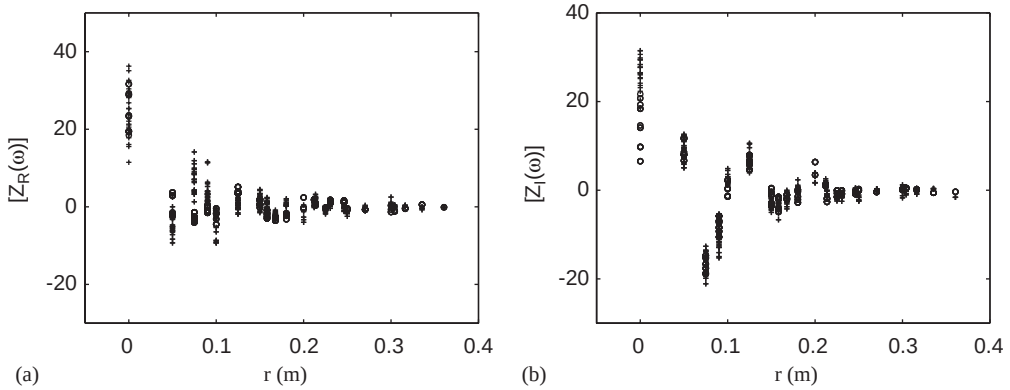

Fig. 9. (a) Real and (b) imaginary parts of the off-diagonal terms of the equivalent acoustic impedance matrix as a function of the distance r at 1396.6086 Hz. Analytical model (circle symbols), experimental results (cross symbols).

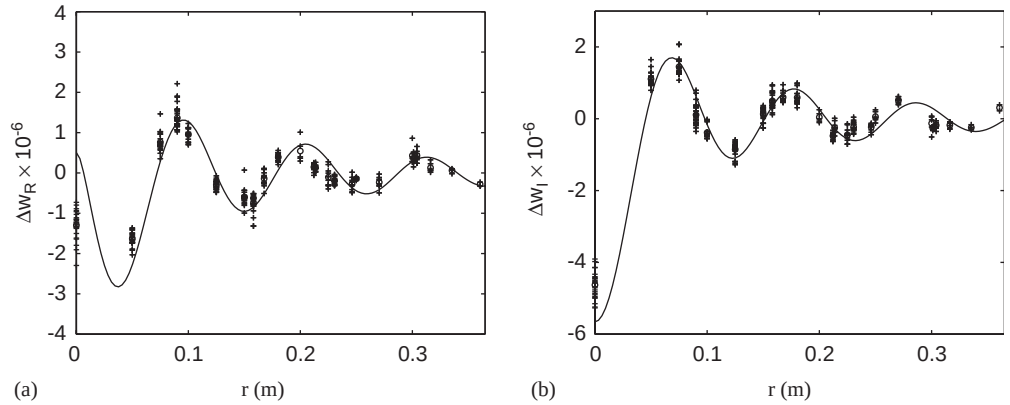

Fig. 10. (a) Real and (b) imaginary parts of the function $r \mapsto \Delta w(r, \omega)$ at the frequency 801.881 Hz for r in [0,0.36] m. Analytical results (solid line), experimental results (cross symbols). Average experimental values over the points having the same distance r (circle symbols).

5.2. Experimental comparisons and validation for the cross-frequency response function

The analytical model of the cross response function between two points distinct of r is the mapping $\omega \mapsto \Delta w(r, \omega)$. In this subsection, one compares the experiments with the analytical results for the function $r \mapsto \Delta w(r, \omega)$ at a fixed frequency equal to 800 Hz. It should be noted that the choice of this frequency is arbitrary, but the quality of the comparisons is similar for any frequency on the frequency band of analysis. Figs. 10(a) and (b) display the graphs of the real and imaginary parts of the function $r \mapsto \Delta w(r, \omega)$ at frequency 800 Hz. The comparisons between the experimental results (cross symbols) and the analytical model (solid line) are good. In addition, in these two figures, the circle symbols correspond to the average of the experimental values over the points having the same distance r.

6. Conclusions

The multilayer system containing porous media is relatively difficult to model in the medium and high frequency domains. The purpose of this paper has been the construction of an analytical expression of the equivalent acoustic impedance for a multilayer system, constituted of a three-dimensional porous medium inserted between two thin plates, for the medium and high frequency ranges. For complex structural acoustic systems, such results can be used to model a soundproofing scheme by a wall acoustic impedance. The methodology proposed can be used to other similar multilayer systems. The boundary value problem of the multilayer system consisting of two-dimensional media (thin plates) coupled with a three-dimensional medium (porous medium) has been presented. The equations for the general case of a homogeneous anisotropic viscoelastic porous medium with homogeneous orthotropic viscoelastic plates have been presented. An analytical model of the equivalent acoustic impedance has been constructed using a spectral method and its validation has been obtained by comparisons with experiments. This construction is not self-evident and an adapted algebraic formulation has to be developed. In the medium and high frequency ranges, the comparisons between the analytical model and the experiments are good enough either for the local impedance or for the cross impedance between the driving and the receiving points. The good agreement of these results gives an experimental validation, firstly, for the mechanical model, i.e., for the boundary value problem, and, secondly, for the analytical method used for the equivalent acoustic impedance. In addition, it should be noted that, similarly to the conclusions given in Part 1 of the paper, the equivalent acoustic impedance tends to be local for frequencies greater than 300 Hz and, in this case, the modulus of this impedance is a quasi exponential decreasing function with the distance.

Acknowledgements

The authors would like to thank ONERA which supports this research.

Appendix A. Expression of the matrices of the matrix equation relative to the porous medium

Substituting constitutive equations (25) and (26) of the porous medium into dynamical equations (20) yields Eq. (34) in which matrices $\mathbb{A}_{11}$, $\mathbb{B}_{11}(\mathbf{k})$, $\mathbb{B}_{12}(\mathbf{k})$, $\mathbb{C}_{11}(\mathbf{k})$, $\mathbb{C}_{12}(\mathbf{k})$ and $\mathbb{C}_{22}(\mathbf{k})$ are defined by

$$\mathbb{A}_{11} = \begin{bmatrix} -B_F/2 & 0 & 0 & 0 \\ 0 & -B_F/2 & 0 & 0 \\ 0 & 0 & -(A_F + B_F) & -C_F \\ 0 & 0 & -C_F & -E_F \end{bmatrix}, \quad \mathbb{B}_{12}(\mathbf{k}) = \begin{bmatrix} 0 & 0 \\ 0 & 0 \\ \mathrm{i}k_1 C_F & \mathrm{i}k_2 C_F \\ \mathrm{i}k_1 E_F & \mathrm{i}k_2 E_F \end{bmatrix},$$

$$\mathbb{B}_{11}(\mathbf{k}) = \begin{bmatrix} 0 & 0 & \mathrm{i}k_1(A_F + B_F/2) & \mathrm{i}k_1 C_F \\ 0 & 0 & \mathrm{i}k_2(A_F + B_F/2) & \mathrm{i}k_2 C_F \\ \mathrm{i}k_1(A_F + B_F/2) & \mathrm{i}k_2(A_F + B_F/2) & 0 & 0 \\ \mathrm{i}k_1 C_F & \mathrm{i}k_2 C_F & 0 & 0 \end{bmatrix},$$

$$\mathbb{C}_{11}(\mathbf{k}) = -\omega^2 \begin{bmatrix} \tilde{\rho}_{11} & 0 & 0 & 0 \\ 0 & \tilde{\rho}_{11} & 0 & 0 \\ 0 & 0 & \tilde{\rho}_{11} & \tilde{\rho}_{12} \\ 0 & 0 & \tilde{\rho}_{12} & \tilde{\rho}_{22} \end{bmatrix} + \mathrm{i}\omega b \begin{bmatrix} 1 & 0 & 0 & 0 \\ 0 & 1 & 0 & 0 \\ 0 & 0 & 1 & -1 \\ 0 & 0 & -1 & 1 \end{bmatrix}$$
$$+ \begin{bmatrix} (A_F + B_F)k_1^2 + B_F k_2^2/2 & k_1 k_2 (A_F + B_F/2) & 0 & 0 \\ k_1 k_2 (A_F + B_F/2) & (A_F + B_F)k_2^2 + B_F k_1^2/2 & 0 & 0 \\ 0 & 0 & (k_1^2 + k_2^2)B_F/2 & 0 \\ 0 & 0 & 0 & 0 \end{bmatrix},$$

$$\mathbb{C}_{12}(\mathbf{k}) = -\omega^2 \tilde{\rho}_{12} \begin{bmatrix} 1 & 0 \\ 0 & 1 \\ 0 & 0 \\ 0 & 0 \end{bmatrix} + \mathrm{i}\omega b \begin{bmatrix} -1 & 0 \\ 0 & -1 \\ 0 & 0 \\ 0 & 0 \end{bmatrix} + C_F \begin{bmatrix} k_1^2 & k_1 k_2 \\ k_1 k_2 & k_2^2 \\ 0 & 0 \\ 0 & 0 \end{bmatrix},$$

$$\mathbb{C}_{22}(\mathbf{k}) = -\omega^2 \tilde{\rho}_{22} \begin{bmatrix} 1 & 0 \\ 0 & 1 \end{bmatrix} + \mathrm{i}\omega b \begin{bmatrix} 1 & 0 \\ 0 & 1 \end{bmatrix} + E_F \begin{bmatrix} k_1^2 & k_1 k_2 \\ k_1 k_2 & k_2^2 \end{bmatrix}.$$

Appendix B. Expression of matrix $\mathbb{M}_H(\mathbf{k},\omega)$ relating vector $(\mathbf{X}'(H),\mathbf{X}'(0))$ with vector $(\mathbf{X}(H),\mathbf{X}(0))$

For $x_3 \in]0,H[$, the matrix $\mathscr{D}(\mathbf{k},x_3)$ has four diagonal terms which are exponentionally increasing and which yields a bad numerical conditioning of the problem. The solution retained consists of splitting $\mathscr{D}(\mathbf{k},x_3)$ into two matrices $\mathbb{D}^+(\mathbf{k},x_3)$ corresponding to the eigenvalues with positive real parts and $\mathbb{D}^-(\mathbf{k},x_3)$ corresponding to the eigenvalues with negative real parts, such that

$$\mathscr{D}(\mathbf{k},x_3) = \begin{bmatrix} \mathbb{D}^+(\mathbf{k},x_3) & 0 \\ 0 & \mathbb{D}^-(\mathbf{k},x_3) \end{bmatrix}$$

$$\text{with} \quad [\mathbb{D}^+(\mathbf{k},x_3)]_{jk} = \delta_{jk} \mathrm{e}^{x_3 \lambda_j^+(\mathbf{k})}, \quad [\mathbb{D}^-(\mathbf{k},x_3)]_{jk} = \delta_{jk} \mathrm{e}^{x_3 \lambda_j^-(\mathbf{k})}.$$

Defining $\mathbf{T}(x_3) = \Phi(\mathbf{k})^{-1}\mathbf{W}(x_3)$, the first equation (39) in $x_3 = H$ can be rewritten as $\mathbf{T}(H) = \mathscr{D}(\mathbf{k},H)\mathbf{T}(0)$. Splitting $\mathbf{T}(x_3) = (\mathbf{T}^+(x_3),\mathbf{T}^-(x_3))$ yields $\mathbf{T}^-(H) = \mathbb{D}^-(\mathbf{k},H)\mathbf{T}^-(0)$ and $\mathbf{T}^+(0) = (\mathbb{D}^+(\mathbf{k},H))^{-1}\mathbf{T}^+(H)$. Introducing the matrix $[\mathbb{D}_-(\mathbf{k},H)]$ such that $[\mathbb{D}_-(\mathbf{k},H)] = [\mathbb{D}^+(\mathbf{k},H)]^{-1}$, ones then has $[\mathbb{D}_-(\mathbf{k},H)]_{jk} = \delta_{jk}\mathrm{e}^{-x_3\lambda_j^+(\mathbf{k})}$ for j and k in $1,\ldots,4$, thus, one obtains

$\mathbf{T}^+(0) = \mathbb{D}_-(\mathbf{k}, H)\mathbf{T}^+(H)$. The matrix $\Phi(\mathbf{k}, x_3)$ can be written as

$$\Phi(\mathbf{k}, x_3) = \begin{bmatrix} \Phi_{++}(\mathbf{k}, x_3) & \Phi_{+-}(\mathbf{k}, x_3) \\ \Phi_{-+}(\mathbf{k}, x_3) & \Phi_{--}(\mathbf{k}, x_3) \end{bmatrix}.$$

Therefore, taking into account the definition of $\mathbf{T}(x_3)$, one obtains

$$\begin{aligned} \mathbf{X}'(H) &= \Phi_{++}(\mathbf{k}, H)\mathbf{T}^+(H) + \Phi_{+-}(\mathbf{k}, H)\mathbf{T}^-(H), \\ \mathbf{X}'(0) &= \Phi_{++}(\mathbf{k}, 0)\mathbf{T}^+(0) + \Phi_{+-}(\mathbf{k}, 0)\mathbf{T}^-(0), \\ \mathbf{X}(H) &= \Phi_{-+}(\mathbf{k}, H)\mathbf{T}^+(H) + \Phi_{--}(\mathbf{k}, H)\mathbf{T}^-(H), \\ \mathbf{X}(0) &= \Phi_{-+}(\mathbf{k}, 0)\mathbf{T}^+(0) + \Phi_{--}(\mathbf{k}, 0)\mathbf{T}^-(0). \end{aligned}$$

Solving these four matrix equations yields a linear mapping between the vector $(\mathbf{X}'(H), \mathbf{X}'(0))$ and the vector $(\mathbf{X}(H), \mathbf{X}(0))$ such as

$$\begin{bmatrix} \mathbf{X}'(H) \\ \mathbf{X}'(0) \end{bmatrix} = \mathbb{M}_H(\mathbf{k}, \omega) \begin{bmatrix} \mathbf{X}(H) \\ \mathbf{X}(0) \end{bmatrix} \quad \text{in which } \mathbb{M}_H(\mathbf{k}, \omega) = \begin{bmatrix} \mathbb{S}_{HH}\mathbb{R}_{HH}^{-1} & \mathbb{S}_{H0} - \mathbb{S}_{HH}\mathbb{R}_{HH}^{-1}\mathbb{R}_{H0} \\ \mathbb{S}_{0H}\mathbb{R}_{HH}^{-1} & \mathbb{S}_{00} - \mathbb{S}_{0H}\mathbb{R}_{HH}^{-1}\mathbb{R}_{H0} \end{bmatrix},$$

and where

$$\begin{aligned} \mathbb{S}_{HH}(\mathbf{k}, 0, H) &= \Phi_{++}(\mathbf{k}, H) - \Phi_{+-}(\mathbf{k}, H)\mathbb{D}^-(\mathbf{k}, H)\Phi_{--}(\mathbf{k}, 0)^{-1}\Phi_{-+}(\mathbf{k}, 0)\mathbb{D}_-(\mathbf{k}, H), \\ \mathbb{R}_{H0}(\mathbf{k}, 0, H) &= \Phi_{--}(\mathbf{k}, H)\mathbb{D}^-(\mathbf{k}, H)\Phi_{--}(\mathbf{k}, 0)^{-1}, \\ \mathbb{R}_{HH}(\mathbf{k}, 0, H) &= \Phi_{-+}(\mathbf{k}, H) - \Phi_{--}(\mathbf{k}, H)\mathbb{D}^-(\mathbf{k}, H)\Phi_{--}(\mathbf{k}, 0)^{-1}\Phi_{-+}(\mathbf{k}, 0)\mathbb{D}_-(\mathbf{k}, H), \\ \mathbb{S}_{H0}(\mathbf{k}, 0, H) &= \Phi_{+-}(\mathbf{k}, H)\mathbb{D}^-(\mathbf{k}, H)\Phi_{--}(\mathbf{k}, 0)^{-1}, \\ \mathbb{S}_{0H}(\mathbf{k}, 0, H) &= \Phi_{++}(\mathbf{k}, 0)\mathbb{D}_-(\mathbf{k}, H) - \Phi_{+-}(\mathbf{k}, 0)\Phi_{--}(\mathbf{k}, 0)^{-1}\Phi_{-+}(\mathbf{k}, 0)\mathbb{D}_-(\mathbf{k}, H), \\ \mathbb{S}_{00}(\mathbf{k}, 0) &= \Phi_{+-}(\mathbf{k}, 0)\Phi_{--}(\mathbf{k}, 0)^{-1}. \end{aligned}$$

It should be noted that $\mathbb{R}_{HH}(\mathbf{k}, 0, H)$ is invertible.

References

[1] P.M. Morse, K.U. Ingard, *Theoretical Acoustics*, Princeton University Press, Princeton, NJ, 1968.
[2] J.D. Achenbach, *Wave Propagation in Elastic Solids*, North–Holland, Amsterdam, 1973.
[3] M. Bruneau, *Introduction aux Théories de l'Acoustique*, Université du Maine, Le Mans, 1993.
[4] F. Fahy, *Sound and Structural Vibration*, Academic Press, London, 1987.
[5] C. Lesueur, *Rayonnement Acoustique des Structures-Vibroacoustique-Intéractions Fluide-structure*, Eyrolles, Paris, 1988.
[6] A. Blaise, C. Lesueur, M. Gotteland, M. Barbe, On sound transmission into an orthotropic infinite shell: comparison with Koval's results and understanding of phenomena, *Journal of Sound and Structural Vibration* 155 (1) (1992) 95–109.
[7] M.C. Junger, D. Feit, *Sound, Structures, and Their Interaction*, Acoustical Society of America, New York, 1993.
[8] A.D. Pierce, *Acoustics—An Introduction to Its Physical Principles and Applications*, 3rd Edition, Acoustical Society of America, New York, 1994.
[9] R. Ohayon, C. Soize, *Structural Acoustics and Vibration*, Academic Press, London, 1998.
[10] J.L. Guyader, C. Lesueur, Acoustic transmission through orthotropic multilayered plates, part I. Plate vibrations modes, *Journal of Sound and Vibration* 58 (1) (1978) 51–68.

[11] G. Maidanik, J. Dickey, Designing a negligible specular reflection coefficient for a panel with a compliant layer, *Journal of the Acoustical Society of America* 90 (4) (1991) 2139–2145.
[12] A. Blaise, C. Lesueur, Acoustic transmission through a 2D orthotropic multilayered infinite cylindrical shell, *Journal of Sound and Vibration* 155 (1) (1992) 95–109.
[13] C. Lesueur, G. Poumerol, A. Blaise, Vibroacoustic response of composite multilayered plate coupled to a rectangular cavity and excited by white noise and a turbulent boundary layer, *Acta Acustica* 3 (2) (1995) 153–167.
[14] J.M. Cushieri, D. Feit, Influence of circumferential partial coating on the acoustic radiation from a fluid-loaded shell, *Journal of the Acoustical Society of America* 107 (6) (2000) 3196–3207.
[15] Y.F. Hwang, M. Kim, P.J. Zoccola, Acoustic radiation by point- or line-excited laminated plates, *Journal of Vibration and Acoustics* 122 (2000) 189–195.
[16] G. Maidanik, J. Dickey, A boundary that sustains a negligible specular reflection coefficient over a wide frequency band, *Journal of the Acoustical Society of America* 107 (3) (2000) 1103–1110.
[17] M.E. Delany, E.N. Bazley, Acoustical properties of fibrous materials, *Applied Acoustics* 3 (1970) 105–116.
[18] D.L. Johnson, J. Koplik, R. Dashen, Theory of dynamic permeability and tortuosity in fluid-saturated porous media, *Journal of Fluid Mechanics* 176 (1987) 379–402.
[19] Y. Champoux, J.F. Allard, Dynamic tortuosity and bulk modulus in air-saturated porous media, *Journal of Applied Physics* 70 (1991) 1975–1979.
[20] C. Zwikker, C.W. Kosten, *Sound Absorbing Materials*, Elsevier, New York, 1949.
[21] T. Bourbie, O. Coussy, B. Zinszner, *Acoustics of Porous Media*, Technip, Paris, 1987.
[22] O. Coussy, *Mécanique des Milieux Poreux*, Technip, Paris, 1991.
[23] M.A. Biot, in: I. Tolstoy (Ed.), *Acoustics, Elasticity and Thermodynamics of Porous Media: Twenty one papers by M.A. Biot*, Acoustical Society of America, New York, 1992.
[24] J.F. Allard, *Propagation of Sound in Porous Media: Modelling Sound Absorbing Materials*, Chapman & Hall, London, 1993.
[25] B.P. Semeniuk, C.L. Morfey, M. Petyt, Revised macroscopic model of sound propagation through a fibrous thermal insulation, ISVR Technical Memorandum No 744, BRAIN Deliverable No 13b, 1994.
[26] B.P. Semeniuk, C.L. Morfey, M. Petyt, Final equations of motion of a fibrous porous material, ISVR Technical Memorandum No 767, BRAIN Deliverable No 13d, 1995.
[27] S. Gorog, R. Panneton, N. Atalla, Mixed displacement-pressure formulation for acoustic anisotropic open porous media, *Journal of Applied Physics* 82 (1997) 4192–4196.
[28] P. Göransson, A 3-D, symmetric, finite element formulation of the Biot equations with applications to acoustic wave propagation through an elastic porous medium, *International Journal of Numerical Methods in Engineering* 41 (1999) 167–192.
[29] N. Atalla, M.A. Hamdi, R. Panneton, Enhanced weak integral formulation for the mixed (u,p) poroelastic equations, *Journal of the Acoustical Society of America* 109 (6) (2001) 3065–3068.
[30] Th. Levy, E. Sanchez Palencia, On boundary conditions for fluid flow in porous media, *International Journal of Engineering Science* 13 (1975) 923–940.
[31] Th. Levy, E. Sanchez Palencia, Equations and interface conditions for acoustic phenomena in porous media, *Journal of Mathematical Analysis and Applications* 61 (1977) 813–834.
[32] B. Gurevich, M. Schoenberg, Interface conditions for Biot's equations of poroelasticity, *Journal of the Acoustical Society of America* 105 (5) (1999) 2585–2589.
[33] Y.J. Kang, J.S. Bolton, Finite element modelling of isotropic elastic porous materials coupled with acoustical finite elements, *Journal of the Acoustical Society of America* 98 (1) (1995) 635–643.
[34] Y.J. Kang, J.S. Bolton, A finite element model for sound transmission through foam-lined double panel structures, *Journal of the Acoustical Society of America* 99 (5) (1996) 2755–2765.
[35] R. Panneton, Modélisation Numérique Tridimensionnelle par Éléments Finis des Milieux Poroélastiques, Ph.D. Thesis, University of Sherbrooke, 1996.
[36] R. Panneton, N. Atalla, Numerical prediction of sound transmission through finite multilayer systems with poroelastic materials, *Journal of the Acoustical Society of America* 100 (1) (1996) 346–354.
[37] R. Panneton, N. Atalla, An efficient finite element scheme for solving the three-dimensional poroelasticity problem in acoustics, *Journal of the Acoustical Society of America* 101 (6) (1997) 3287–3298.

[38] N. Atalla, R. Panneton, P. Debergue, A mixed displacement-pressure formulation for poroelastic materials, *Journal of the Acoustical Society of America* 104 (3) (1998) 1444–1452.
[39] N. Dauchez, Etude Vibroacoustique des Matériaux Poreux par Éléments Finis, Ph.D. Thesis, University of Maine-University of Sherbrooke, 1999.
[40] M.A. Hamdi, N. Atalla, L. Mebarek, A. Omrani, Novel mixed finite element formulation for the analysis of sound absorption by porous materials, *Inter Noise 2000*, 29*th International Congress and Exhibition on Noise Control Engineering*, Nice, August 2000.
[41] F.C. Sgard, N. Atalla, J. Nicolas, A numerical model for the low-frequency diffuse field sound transmission loss of double-wall sound barriers with elastic porous linings, *Journal of the Acoustical Society of America* 108 (6) (2000) 2865–2872.
[42] J.F. Allard, A. Aknine, C. Depollier, Acoustical properties of partially reticulated foams with high and medium flow resistance, *Journal of the Acoustical Society of America* 79 (6) (1986) 1734–1740.
[43] J.F. Allard, Y. Champoux, C. Depollier, Modelization of layered sound absorbing materials with transfert matrices, *Journal of the Acoustical Society of America* 82 (5) (1987) 1792–1796.
[44] J.S. Bolton, N.M. Shiau, Oblique incidence sound transmission through multi-panel structures lined with elastic porous materials, *AIAA* 11*th Aeroacoustics Conference*, Palo Alto, October 1987, Paper AIAA-87-2660.
[45] W. Lauriks, A. Cops, J.F. Allard, C. Depollier, P. Rebillard, Modelization at oblique incidence of layered porous materials with impervious screens, *Journal of the Acoustical Society of America* 87 (3) (1990) 1200–1206.
[46] W. Lauriks, P. Mees, J.F. Allard, The acoustic transmission through layered systems, *Journal of Sound and Vibration* 155 (1) (1992) 125–132.
[47] J.S. Bolton, N.M. Shiau, Y.J. Kang, Sound transmission through multi-panel structures lined with elastic porous materials, *Journal of Sound and Vibration* 191 (3) (1996) 317–347.
[48] B.H. Song, J.S. Bolton, A transfer-matrix approach for estimating the characteristic impedance and wave numbers of limp and rigid porous materials, *Journal of the Acoustical Society of America* 107 (3) (2000) 1131–1152.
[49] B. Faverjon, C. Soize, Equivalent acoustic impedance model. Part 1: experiments and semi-physical model, *Journal of Sound and Vibration* 276 (3–5) (2004) 571–592, this issue.
[50] J.A. Arango, L.P. Lebedev, Some boundary value problems and models for coupled elastic bodies, *Quarterly of Applied Mathematics* 56 (1) (1998) 157–172.
[51] B. Faverjon, Modélisation et Validation Expérimentale d'un Modèle d'Impédance Acoustique dans le Domaine des Moyennes et Hautes Fréquences pour un Système Multicouche Composé d'un Matériau Poreux Épais Inséré entre Deux Plaques Minces, Thèse de Doctorat, Conservatoire National des Arts et Métiers, 2002.
[52] N. Dauchez, Characterization of a poroelastic material, CTTM-ONERA Report, 2001 (in French).
[53] L. Guillaumie, Wall acoustic impedance. Experimental identification, ONERA Report, No RTS 2/03239 DDSS, 2001 (in French).